Nanoscale

PAPER

View Article Online
View Journal | View Issue

Cite this: *Nanoscale*, 2016, **8**, 6666

Nonlinear spectral and lifetime management in upconversion nanoparticles by controlling energy distribution†

Yu Wang,[a] Renren Deng,[a] Xiaoji Xie,[b] Ling Huang*[b] and Xiaogang Liu*[a,c,d]

Received 29th January 2016,
Accepted 24th February 2016

DOI: 10.1039/c6nr00812g

www.rsc.org/nanoscale

Optical tuning of lanthanide-doped upconversion nanoparticles has attracted considerable attention over the past decade because this development allows the advance of new frontiers in energy conversion, materials science, and biological imaging. Here we present a rational approach to manipulating the spectral profile and lifetime of lanthanide emission in upconversion nanoparticles by tailoring their nonlinear optical properties. We demonstrate that the incorporation of energy distributors, such as surface defects or an extra amount of dopants, into a rare-earth-based host lattice alters the decay behavior of excited sensitizers, thus markedly improving the emitters' sensitivity to excitation power. This work provides insight into mechanistic understanding of upconversion phenomena in nanoparticles and also enables exciting new opportunities of using these nanomaterials for photonic applications.

Introduction

Lanthanide-doped photon upconversion materials have been studied for several decades owing to their distinct optical properties such as large anti-Stokes' spectral shift, long luminescence lifetime, and sharp emission band. These attributes make the upconversion materials particularly attractive for use in lighting, lasing, quantum cutting, *etc*.[1,2] In recent years, the rapid development of nanotechnology has enabled immense interest in upconversion nanoparticles (UCNPs) because of their fascinating optical properties and technological potential in many fields of research.[3–37] Notably, many strategies, including doping composition/concentration variation, surface ligand coordination and pulse-duration modulation, have been developed to tune the emission profile of the UCNPs.[38–45] An important and facile route to control upconversion emission, based on the nonlinear power response of photon upconversion, is to vary the excitation power externally.[46–48]

In a typical photon upconversion process, the excitation energy is absorbed by sensitizers, such as Yb^{3+} ions doped in a host matrix, and then transferred to neighboring emitters (or activators), such as Er^{3+} or Tm^{3+} featuring ladder-like energy states (Fig. S1 in the ESI†). The sequential photon absorption by the sensitizers permits the emitters to be excited to higher energy levels through energy transfer. It is widely accepted that for multi-step (n) energy transfer, the luminescence intensity I is proportional to n power of the excitation density P.[49,50] Thus, the number of energy transfer upconversion (ETU) steps can be derived from the slope (I–P slope) of the luminescence intensity curve plotted against pump power density in a double-logarithmic representation (Fig. S2†). However, the upconversion emission intensity I may not be strictly proportional to n power of the excitation density P. The n value is likely to be affected by a multitude of factors related to energy distribution in UCNPs, such as a crystalline structure, particle size, and dopant concentration. Moreover, the variation of the n value is typically accompanied by a concurrent change in luminescence decay lifetime, meaning that n is highly relevant to the spectral properties and the luminescence dynamics of upconversion materials.

In this work, we investigate the spectroscopic properties and decay behaviors of UCNPs under the influence of different types of energy distributors through surface defect engineering or doping (Fig. 1). Our measured n value correlates well with upconversion emission characteristics in that large numbers of energy distributing pathways increase the sensitivity of the

[a]*Department of Chemistry, National University of Singapore, Singapore 117543, Singapore. E-mail: chmlx@nus.edu.sg*
[b]*Key Laboratory of Flexible Electronics, Institute of Advanced Materials, Jiangsu National Synergetic Innovation Center for Advanced Materials, Nanjing Tech University, Nanjing 211816, China. E-mail: iamlhuang@njtech.edu.cn*
[c]*Center for Functional Materials, NUS (Suzhou) Research Institute, Suzhou, Jiangsu 215123, China*
[d]*SZU-NUS Collaborative Innovation Center for Optoelectronic Science & Technology, Key Laboratory of Optoelectronic Devices and Systems of Ministry of Education and Guangdong Province, College of Optoelectronic Engineering, Shenzhen University, Shenzhen 518060, China*
†Electronic supplementary information (ESI) available. See DOI: 10.1039/c6nr00812g

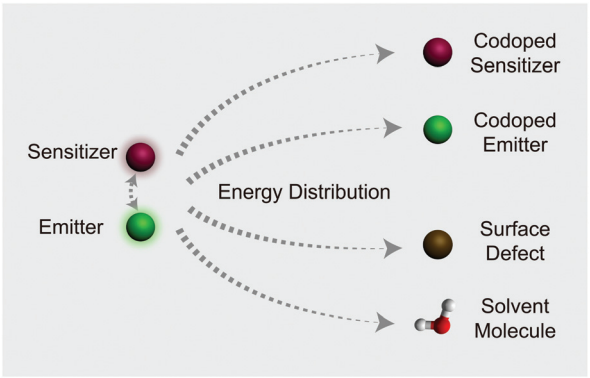

Fig. 1 Illustration of typical energy distribution processes involving Yb^{3+}-sensitized upconversion. Note that for a particular system at the excited state, possible energy distributors include sensitizer ions, codoped emitters, surface defects, and solvent molecules with high energy vibrational groups.

UCNPs to excitation power. Importantly, the decay lifetimes of both sensitizer and emitter ions could be tuned by manipulating the nature of the energy distributors, providing new opportunities for photonic applications in optical switching and security encoding.

Results and discussion

We prepared $NaYF_4$:Yb/Er (20/2%) UCNPs as a model sample by a well-established co-precipitation method.[51] As seen under a transmission electron microscope (TEM), the as-synthesized nanoparticles are 15.3 ± 1.1 nm in diameter with a narrow size distribution (Fig. 2a and b). A pure hexagonal phase structure of the nanoparticles was confirmed by X-ray diffraction studies (Fig. 2c). Under the excitation of a 975 nm CW laser, we observed visible emission bands at 540 and 654 nm, typically attributable to the $^4S_{3/2} \rightarrow {}^4I_{15/2}$ and $^4F_{9/2} \rightarrow {}^4I_{15/2}$ transitions of Er^{3+} ions (Fig. 2d). We considered the 540 nm emission as an example to study the excitation power response and decay behaviors of the UCNPs. The power dependent luminescence measurement indicates that in the power density range of 29–70 W cm^{-2}, the 540 nm emission is generated *via* a typical 2-photon upconversion process (Fig. 2e). On 975 nm pulsed laser excitation, we observed a distinct rise edge in the temporal luminescence curve of the 540 nm emission due to the time consumed by the multi-step energy transfer process.[52] We focus on the decay lifetime of the luminescence which is critical to the application of upconversion tuning in the time domain for optical multiplexing.[9,23] Notably, the emission of Yb^{3+} ($^2F_{5/2} \rightarrow {}^2F_{7/2}$ transition) at 985 nm has a decay lifetime of

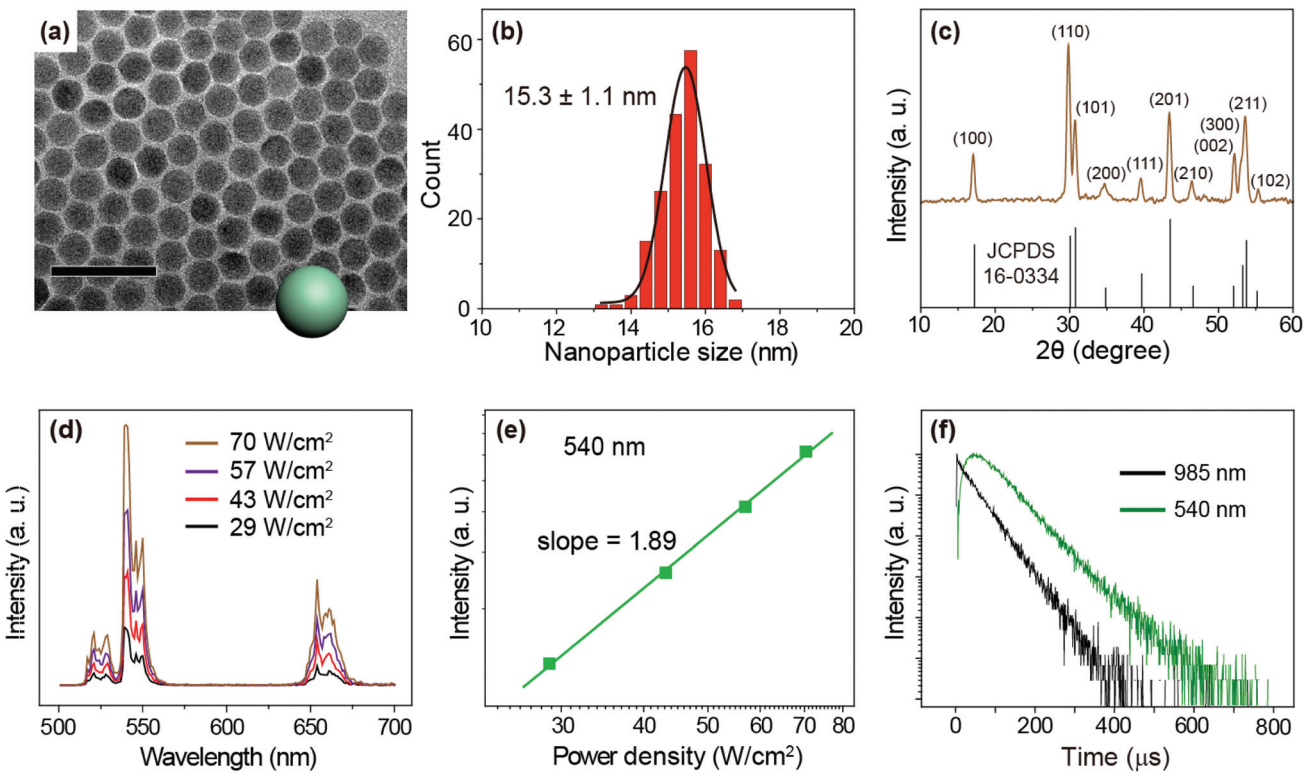

Fig. 2 (a) A typical TEM image of the as-prepared $NaYF_4$:Yb/Er (20/2%) nanoparticles. Scale bar is 50 nm. (b) Size histogram of the nanoparticles. (c) X-ray diffraction patterns of the nanoparticles, which are in good agreement with the literature reference for hexagonal $NaYF_4$ crystal (Joint Committee on Powder Diffraction Standards file number 16-0334). (d) Emission spectra of the UCNPs recorded with a 975 nm CW laser excitation at different power densities (29–70 W cm^{-2}). (e) The 540 nm ($^4S_{3/2} \rightarrow {}^4I_{15/2}$ transition of Er^{3+}) emission intensity *versus* pump power density in double-logarithmic representation. (f) Decay curves of 540 nm emissions from Er^{3+} as well as 985 nm from Yb^{3+} obtained upon excitation of the nanoparticles at 975 nm.

69 μs, while the decay of Er^{3+} emission at 540 nm registers a lifetime of 88 μs (Fig. 2f).

To study the change in the *I–P* slope and emission lifetime in the presence of varied energy distributors, we adopted different strategies to alter the upconversion luminescence of $NaYF_4$:Yb/Er (20/2%) UCNPs: (i) surface passivation by coating the particles with different thicknesses of a $NaYF_4$ inert shell (Fig. S3†);[53–60] (ii) controlling the size of UCNPs (Fig. S4†);[61] (iii) coating the particles with a $NaYF_4$:Yb active shell containing different amounts of Yb^{3+} (Fig. S6†);[62,63] and (iv) changing the Er^{3+} doping concentrations (Fig. S7†). By investigating the luminescence decay lifetime and the pump-power-dependent luminescence intensity as shown in Table 1, it is evident that the *I–P* slopes of the 540 nm emission enlarge with increasing numbers of energy distributors, indicating the high sensitivity of the luminescence to the excitation power density. Notably, the luminescence decay lifetimes of both Yb^{3+} and Er^{3+} are found to diminish as the number of energy distributors increases.

In addition, high levels of vibration energy in solvent molecules are considered to be a dominant factor governing the luminescence profiles of UCNPs. As can be seen in Fig. S8,† ligand-free $NaYF_4$:Yb/Tm (30/0.5%) nanoparticles showed a short decay lifetime (346 μs) in water and a large *I–P* slope for Tm^{3+} emission at 800 nm. Indeed, the high vibration nature of water molecules allows the multiphonon relaxation process to be more accessible.[64] It is worth noting that with the coating of $NaYF_4$ the core–shell nanoparticles showed essentially the same decay lifetime and *I–P* slope in cyclohexane and water. Taken together, our results suggest that the vast combinations of different energy distributors (such as surface defects, dopants and solvents) enable precise depletion of the excited states of Yb^{3+} ions, thereby allowing the emission decay lifetime of the nanoparticles to be controlled within a wide range (Table 1). These strategies could be utilized in generating distinct time-domain codes for optical multiplexing and security applications. Another important note is that without the sensitizer the influence of energy distributors on the luminescence properties of the emitter is virtually negligible (Fig. S9†).

The effect of energy distributors on the measured decay lifetime of Yb^{3+} is investigated using the rate equations derived from a sensitization upconversion model (Fig. 3):

$$\tau = \frac{1}{\sum W_i N_i + W_D N_D + R_b} \quad (1)$$

where N_i (i = 0, 1, 2...) is the population density of the emitter on level i and W_i is the corresponding energy transfer rate from the sensitizer to the emitter. W_D is the energy transfer rate from the sensitizer to the energy distributor. N_D represents the population density of effective energy distributors. R_b is the radiative decay rate of the sensitizer from the excited state. From eqn (1), one can conclude that increasing the number of energy distributors accelerates the depletion of excited Yb^{3+} ions and thus shortens the measured Yb^{3+} decay lifetime.

We next carried out theoretical investigations to explore the fundamental principle underlying the spectral and lifetime management of UCNPs through the control of energy distribution within the particles. From the analysis of the rate equations of energy levels in a simplified two-photon upconversion process (see the ESI†), the population density at the emitting level N_2, which is proportional to the emission intensity I, can be expressed by eqn (2):

$$N_2 = \frac{{N_b}^2}{A \cdot N_b + B} \quad (2)$$

Table 1 Comparative investigations of emission profiles for different types of nanoparticles. Note that decay lifetimes were measured at 985 and 540 nm, and the *I–P* slope tuning was realized by modulating energy distributors through a variety of strategies, including inert and active shell coating, particle size control, and doping concentration adjustment. All 540 nm *I–P* slopes were measured under CW laser excitation at 975 nm with a power density range of 20–80 W cm^{-2}

Structure	Core composition	Core diameter (nm)	Shell composition	Shell thickness (nm)	985 nm (μs)	540 nm (μs)	540 nm *I–P* slope
UCNPs with different inert shells	$NaYF_4$:Yb/Er (20/2%)	15.3	—	—	69	88	1.89
	$NaYF_4$:Yb/Er (20/2%)	15.3	$NaYF_4$	1.3	304	187	1.77
	$NaYF_4$:Yb/Er (20/2%)	15.3	$NaYF_4$	1.8	403	251	1.73
	$NaYF_4$:Yb/Er (20/2%)	15.3	$NaYF_4$	2.8	783	301	1.63
UCNPs with different sizes	$NaYF_4$:Yb/Er (20/2%)	15.3	—	—	69	88	1.89
	$NaYF_4$:Yb/Er (20/2%)	23.8	—	—	327	245	1.76
	$NaYF_4$:Yb/Er (20/2%)	27.2	—	—	506	333	1.65
UCNPs with different active shells	$NaYF_4$:Yb/Er (20/2%)	15.3	$NaYF_4$	1.6	379	231	1.74
	$NaYF_4$:Yb/Er (20/2%)	15.3	$NaYF_4$:Yb (10%)	1.9	274	180	1.78
	$NaYF_4$:Yb/Er (20/2%)	15.3	$NaYF_4$:Yb (20%)	1.7	131	128	1.82
UCNPs with different emitter concentrations	$NaYF_4$:Yb/Er (20/0.5%)	15.3	—	—	101	123	1.83
	$NaYF_4$:Yb/Er (20/1%)	15.5	—	—	97	103	1.88
	$NaYF_4$:Yb/Er (20/2%)	15.3	—	—	69	88	1.89
	$NaYF_4$:Yb/Er (20/4%)	15.7	—	—	50	65	1.92
	$NaYF_4$:Yb/Er (20/8%)	15.2	—	—	35	34	1.92
	$NaYF_4$:Yb/Er (20/16%)	15.2	—	—	19	14	1.98
	$NaYF_4$:Yb/Er (20/32%)	15.4	—	—	13	7	2.09

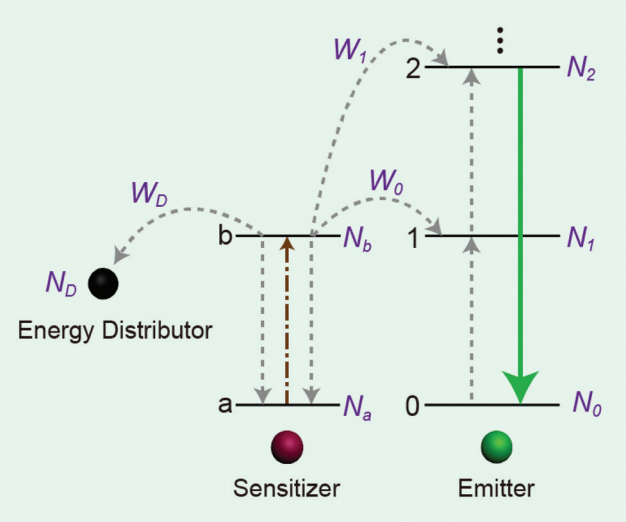

Fig. 3 Simplified scheme of the energy distributor effect on energy transfer processes involving a sensitization upconversion mechanism.

where A and B are constants, N_b denotes the population density of the excited states of the Yb^{3+} sensitizer, which determines the population density of the emitting level. From eqn (2), the N_2–N_b slope value in double-logarithmic representation is calculated in between 1 and 2.[50] Upon excitation with a power density of P, N_b can be further derived from eqn (3):

$$N_b = \frac{P}{C + D \cdot P} \quad (3)$$

where C and D are constants. Notably, N_b is not simply proportional to the excitation power density P, as indicated in eqn (3). We conducted numerical simulations on $NaYF_4$:Yb/Er (20/2%) UCNPs to validate the relationship of N_b with the incident photon flux by introducing the rate equations of a two-photon upconversion process, as shown in Fig. 4a. We consider that the population density of Yb^{3+} at the excited state is nonlinear to the excitation photon flux due to the excitation saturation of Yb^{3+}. This phenomenon further affects the relationship of N_2–P, resulting in the deviation of the I–P slope away from the normal range. Our numerical simulations on both $NaYF_4$:Yb/Er (20/2%) and $NaYF_4$:Yb/Er (20/2%)@$NaYF_4$ (~2.8 nm in shell thickness) UCNPs indicated that the slope of N_2–P diminishes with increasing excitation photons. Compared with the core particles, the shell-coated UCNPs showed a lower value of the I–P slope under identical incident photon flux (Fig. 4b). Remarkably, the simulated value of the I–P slope could be reduced to less than 1 at a high power excitation, which agrees well with our experimental results (Fig. 4c).

From published work, it can be found that in Yb^{3+}/Er^{3+}/Tm^{3+} triply-doped upconversion systems, increasing the excitation power density of UCNPs give rise to a larger rate of increase in the blue emission intensity than that of the green emission intensity.[46,65–68] This can be attributed to the fact that blue emission from Tm^{3+} ($^1G_4 \rightarrow {}^3H_6$ and $^1D_2 \rightarrow {}^3F_4$ transitions) requires more excited photons than green emission from Er^{3+} ($^2H_{11/2}/{}^4S_{3/2} \rightarrow {}^4I_{15/2}$ transitions) (Fig. S1†). As a result, the blue emission typically features a large I–P slope n, thus its intensity increases rapidly with increasing excitation power density. On the basis of the findings described in

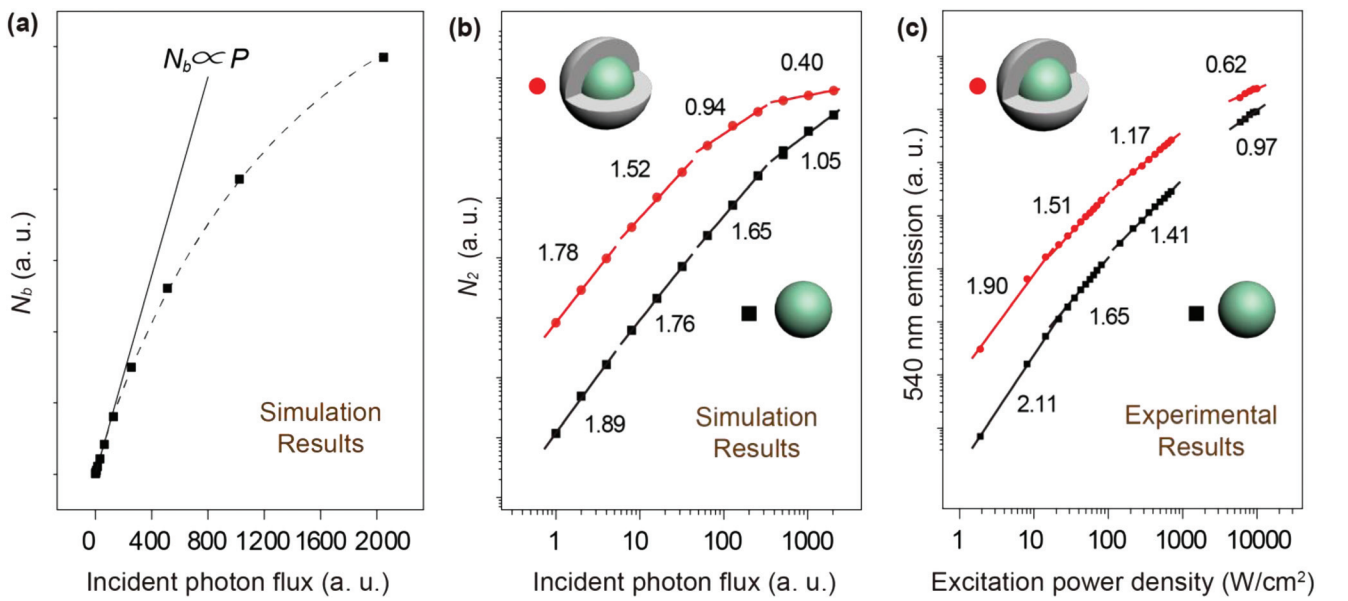

Fig. 4 (a) Numerical simulations on the population density of the excited state of Yb^{3+} ions *versus* the number of excitation photon flux in linear representation using $NaYF_4$:Yb/Er (20/2%) UCNPs. (b) Numerical simulations on the population density of the 540 nm emission level of Er^{3+} ions *versus* the number of excitation photon flux in double-logarithmic representation using $NaYF_4$:Yb/Er (20/2%) and $NaYF_4$:Yb/Er (20/2%)@$NaYF_4$ (~2.8 nm in shell thickness) core–shell UCNPs. (c) Power-density-dependent emission profiles of $NaYF_4$:Yb/Er (20/2%) and $NaYF_4$:Yb/Er (20/2%)@$NaYF_4$ core–shell UCNPs at 540 nm. The excitation power density under study is in the range of 1–10^4 W cm^{-2}.

Table 1, we reason that placing the emitters in regions close to energy distributors, for example, at the particle surface, might be able to improve the particle's sensitivity to the excitation power density (Fig. 5).

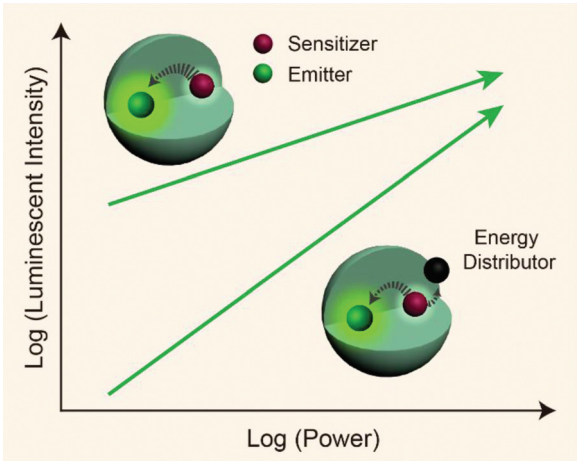

Fig. 5 Schematic representation showing pump-power-dependent luminescence of a sensitizer/emitter codoped nanoparticle in the presence or absence of an energy distributor.

To verify our hypothesis, we prepared two sets of multi-shell structured UCNPs comprising $NaYF_4$:Yb/Tm@$NaYF_4$@$NaYF_4$:Yb/Er@$NaYF_4$:Yb and $NaYF_4$:Yb/Er@$NaYF_4$@$NaYF_4$:Yb/Tm@$NaYF_4$:Yb (Fig. 6a, d and S10†). Note that Tm^{3+} and Er^{3+} ions are doped at different layers for direct comparison of their power-dependent emission profiles. An inert layer of $NaYF_4$ was inserted between the two emitting layers to minimize cross-relaxation between Er^{3+} and Tm^{3+} (Fig. S12 and S13†).[69,70] The outermost $NaYF_4$:Yb shell was utilized to enhance the emission of the outer emitting layer to a level comparable to that obtained from the inner emitting layer (Fig. S14†). As expected, from the obtained emission spectra (Fig. 6b and e), it can be seen that the changes in the blue-to-green emission ratio of these two samples are dramatically different as a function of excitation power density (Fig. 6c, f, and S15a and c†). Consequently, the two colloidal samples exhibited different CIE color profiles with varied excitation power densities (Fig. S15b and d†). As control experiments, we synthesized two similar sets of UCNPs except for replacing the outermost layer of $NaYF_4$:Yb with $NaYF_4$. Interestingly, we observed that both the samples exhibit a similar trend in the blue-to-green emission intensity ratio as measured in response to different excitation powers (Fig. 7). This observation was largely attributed to the elimination of the surface quenching effect through the use of an optically inert $NaYF_4$ layer.

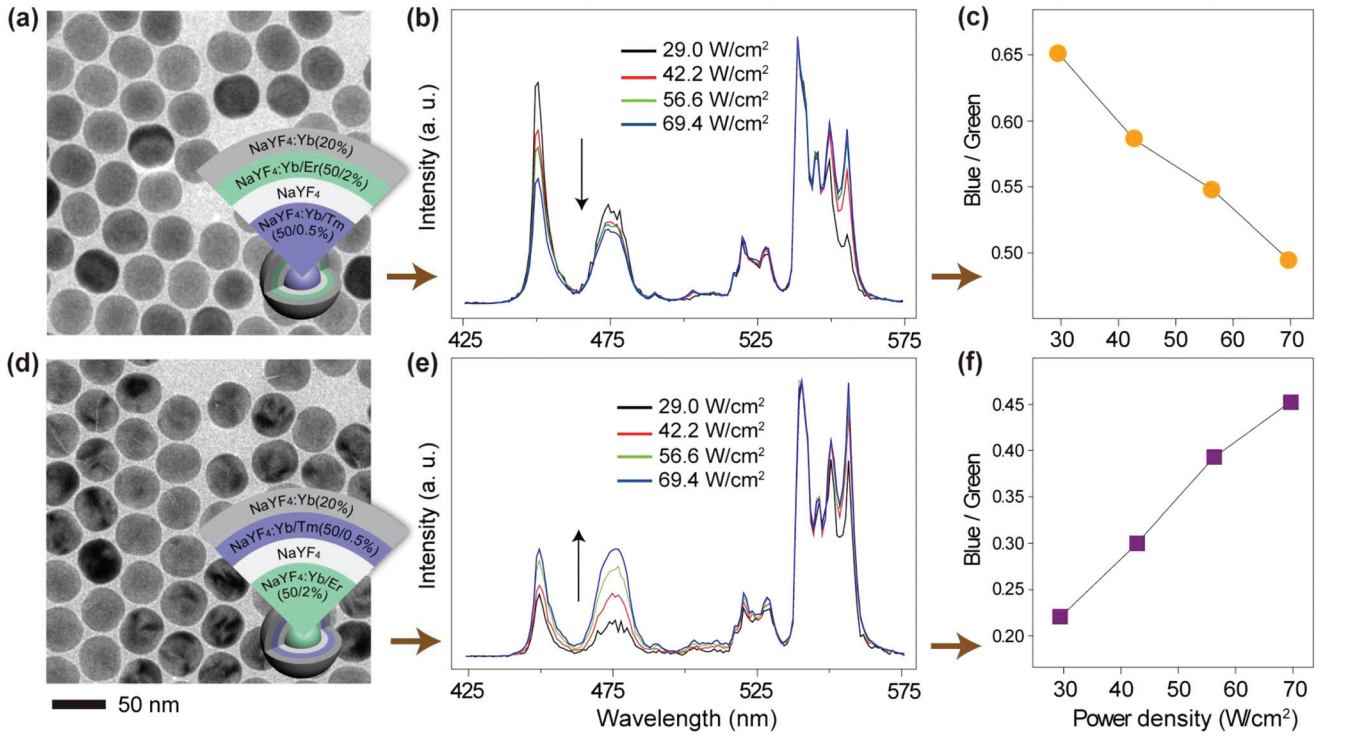

Fig. 6 (a and d) TEM images of $NaYF_4$:Yb/Tm@$NaYF_4$@$NaYF_4$:Yb/Er@$NaYF_4$:Yb and $NaYF_4$:Yb/Er@$NaYF_4$@$NaYF_4$:Yb/Tm@$NaYF_4$:Yb nanoparticles, respectively. Insets showing the design layout of the core–shell structures. (b and e) Corresponding power-dependent upconversion emission spectra of the two samples under 975 nm excitation. (c and f) Corresponding pump-power-dependence of the blue/green emission ratio obtained from the two samples.

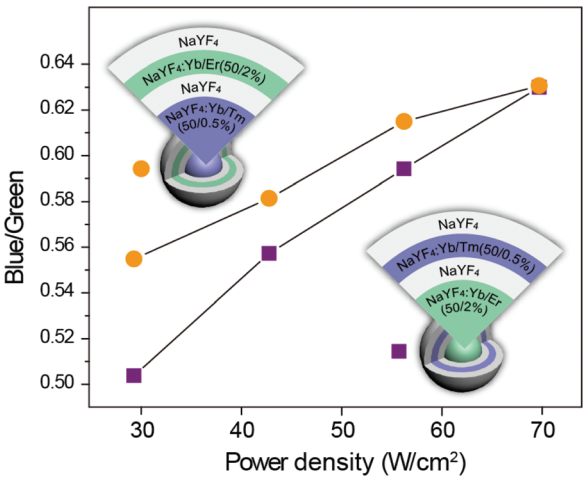

Fig. 7 Power dependent blue-to-green upconversion emission intensity ratio of $NaYF_4$:Yb/Tm@$NaYF_4$@$NaYF_4$:Yb/Er@$NaYF_4$ and $NaYF_4$:Yb/Er@$NaYF_4$@$NaYF_4$:Yb/Tm@$NaYF_4$ UCNPs upon 975 nm laser irradiation.

Conclusions

We have demonstrated a general approach for the design of upconversion nanocrystals with emitters amenable to nonlinear spectral and lifetime management. By controlling the proximity of energy distributors to specific emitters in core–shell structured nanocrystals, power dependent upconversion processes are demonstrated with high temporal tunability. The luminescence lifetime of upconversion nanocrystals can be modified in a wide range, which has potential wide-ranging implications for time-domain optical multiplexing and security applications.

Experimental section

Materials

Yttrium(III) acetate hydrate (99.9%), ytterbium(III) acetate hydrate (99.9%), thulium acetate hydrate (99.9%), erbium(III) acetate hydrate (99.9%), sodium hydroxide (NaOH; >98%), ammonium fluoride (NH_4F; >98%), 1-octadecene (90%), oleic acid (90%), and hydrochloric acid were all purchased from Sigma-Aldrich and used as received without further purification. Analytical grades of ethanol and cyclohexane were purchased from Sigma-Aldrich. Water used in the experiment was purified to have a resistivity of 18.2 MΩ.

Synthesis of $NaREF_4$ (RE = Y, Yb, Tm, Er) core nanoparticles

In a typical experiment,[51] to a 50 mL flask charged with 3 mL of oleic acid (OA) and 7 mL of 1-octadecene (ODE) was added 2 mL of an aqueous solution containing $RE(CH_3CO_2)_3$ precursors with a total lanthanide amount of 0.4 mmol. The resulting mixture was heated at 150 °C for 1 h to form a transparent solution and then cooled down to 50 °C. Subsequently, a methanol solution (6 mL) of NH_4F (1.6 mmol) and NaOH (1 mmol) was added and stirred for 30 min. The reaction temperature was then increased to 110 °C for another 30 min to remove the methanol from the reaction mixture. After that, the solution was heated to 290 °C and maintained at this temperature under an argon atmosphere for 1.5 h. Then the mixture was cooled down to room temperature. The resulting nanoparticles were precipitated out through addition of ethanol, collected by centrifugation (5000 rpm, 10 min), washed with ethanol twice, and finally dispersed in 4 mL of cyclohexane.

Synthesis of $NaREF_4$@$NaREF_4$ (RE = Y, Yb, Tm, Er) core–shell nanoparticles

The shell precursor was prepared by mixing $RE(CH_3CO_2)_3$ (0.2 mmol, RE = Y, Yb, Er, Tm), 3 mL OA and 7 mL ODE in a 50 mL flask, followed by heating at 150 °C for 1 h. After cooling down to 80 °C, 0.2 mmol of $NaREF_4$ core nanoparticles dispersed in 2 mL of cyclohexane was added. The mixture was slowly cooled down to 50 °C for 30 min, and a methanol solution (3 mL) of NH_4F (0.8 mmol) and NaOH (0.5 mmol) was added. Subsequently, the reaction temperature was increased to 110 °C and kept for 30 min to remove the methanol. After that, the solution was heated to 290 °C and maintained at this temperature under an argon flow for 1.5 h. After cooling to room temperature, the nanoparticles were precipitated out by addition of ethanol, collected by centrifugation, washed with ethanol, and redispersed in 4 mL of cyclohexane. The preparation of multi-shell nanoparticles was carried out by repeating the same procedure except for changing the composition ratio of the lanthanides.

Synthesis of ligand-free nanoparticles

The as-prepared OA-capped nanoparticles were dispersed in the mixture containing 1 mL of ethanol and 1 mL of 0.2 M HCl solution. After removal of the surface ligands by sonication for 1 min, the resulting products were collected by centrifugation (14 000 rpm, 20 min) and were re-dispersed in H_2O after washing with a mixed ethanol–H_2O solution (1 : 1, v/v) 3 times.

Characterization

Transmission Electron Microscopy (TEM) measurements were carried out on a JEOL-1400 transmission electron microscope (JEOL) operating at an acceleration voltage of 100 kV. Powder X-ray Diffraction (XRD) data were obtained on a Siemens D5005 X-ray diffractometer with Cu Kα radiation (λ = 1.5406 Å). The upconversion luminescence spectra under 975 nm excitation were recorded using an Edinburgh FSP920-C spectrometer equipped with a photomultiplier (PMT), in conjunction with a 975 nm diode laser (1 W). The CW laser beam was applied onto UCNP samples loaded in a quartz cuvette with a path length of 1 cm. The emission from the samples was collected at an angle of 90° to the excitation beam by using a pair of lenses. The decay curves of upconversion emission were measured by using a customized phosphorescence lifetime spectrometer (FSP920-C, Edinburgh) equipped with a nanosecond optical parametric oscillator (OPO) pumped by using a

3.8-ns-pulsed Nd:YAG laser as the excitation source (Ekspla, NT352).

Acknowledgements

The work was supported in part by the Singapore Ministry of Education (grant no. R143000627112), the GSK (Singapore) Research Fund (R143000492592), the National Natural Science Foundation of China (grant no. 21471109 and 21371095), and the Natural Science Foundation of Jiangsu Province (Key Project: BE2015699, BK20131404, and BL2014075).

Notes and references

1 F. Auzel, *Chem. Rev.*, 2004, **104**, 139–173.
2 S. V. Eliseeva and J.-C. G. Bünzli, *New J. Chem.*, 2011, **35**, 1165.
3 M. Haase and H. Schafer, *Angew. Chem., Int. Ed.*, 2011, **50**, 5808–5829.
4 H. Schäfer, P. Ptacek, B. Voss, H. Eickmeier, J. Nordmann and M. Haase, *Cryst. Growth Des.*, 2010, **10**, 2202–2208.
5 M. Bettinelli, L. Carlos and X. Liu, *Phys. Today*, 2015, **68**, 38–44.
6 N. J. Greybush, M. Saboktakin, X. Ye, C. Della Giovampaola, S. J. Oh, N. E. Berry, N. Engheta, C. B. Murray and C. R. Kagan, *ACS Nano*, 2014, **8**, 9482–9491.
7 W. Yang, X. Li, D. Chi, H. Zhang and X. Liu, *Nanotechnology*, 2014, **25**, 482001.
8 S. Guo, X. Xie, L. Huang and W. Huang, *ACS Appl. Mater. Interfaces*, 2016, **8**, 847–853.
9 W. Zheng, P. Huang, D. Tu, E. Ma, H. Zhu and X. Chen, *Chem. Soc. Rev.*, 2015, **44**, 1379–1415.
10 D. Liu, X. Xu, Y. Du, X. Qin, Y. Zhang, C. Ma, S. Wen, W. Ren, E. M. Goldys, J. A. Piper, S. Dou, X. Liu and D. Jin, *Nat. Commun.*, 2016, **7**, 10254.
11 J. Lai, Y. Zhang, N. Pasquale and K. B. Lee, *Angew. Chem., Int. Ed.*, 2014, **53**, 14419–14423.
12 J. Zhou, Q. Liu, W. Feng, Y. Sun and F. Li, *Chem. Rev.*, 2015, **115**, 395–465.
13 X. Chen, L. Jin, W. Kong, T. Sun, W. Zhang, X. Liu, J. Fan, S. F. Yu and F. Wang, *Nat. Commun.*, 2016, **7**, 10304.
14 B. Zhou, B. Shi, D. Jin and X. Liu, *Nat. Nanotechnol.*, 2015, **10**, 924–936.
15 G. Chen, H. Qiu, P. N. Prasad and X. Chen, *Chem. Rev.*, 2014, **114**, 5161–5214.
16 Y. I. Park, K. T. Lee, Y. D. Suh and T. Hyeon, *Chem. Soc. Rev.*, 2015, **44**, 1302–1317.
17 D. Ni, J. Zhang, W. Bu, H. Xing, F. Han, Q. Xiao, Z. Yao, F. Chen, Q. He, J. Liu, S. Zhang, W. Fan, L. Zhou, W. Peng and J. Shi, *ACS Nano*, 2014, **8**, 1231–1242.
18 A. B. Chinen, C. M. Guan, J. R. Ferrer, S. N. Barnaby, T. J. Merkel and C. A. Mirkin, *Chem. Rev.*, 2015, **115**, 10530–10574.
19 L. L. Li and Y. Lu, *J. Am. Chem. Soc.*, 2015, **137**, 5272–5275.
20 C. Liu, Z. Gao, J. Zeng, Y. Hou, F. Fang, Y. Li, R. Qiao, L. Shen, H. Lei, W. Yang and M. Gao, *ACS Nano*, 2013, **7**, 7227–7240.
21 X. Ai, C. J. Ho, J. Aw, A. B. Attia, J. Mu, Y. Wang, X. Wang, Y. Wang, X. Liu, H. Chen, M. Gao, X. Chen, E. K. Yeow, G. Liu, M. Olivo and B. Xing, *Nat. Commun.*, 2016, **7**, 10432.
22 Y. F. Wang, G. Y. Liu, L. D. Sun, J. W. Xiao, J. C. Zhou and C. H. Yan, *ACS Nano*, 2013, **7**, 7200–7206.
23 Y. Q. Lu, J. B. Zhao, R. Zhang, Y. J. Liu, D. M. Liu, E. M. Goldys, X. S. Yang, P. Xi, A. Sunna, J. Lu, Y. Shi, R. C. Leif, Y. J. Huo, J. Shen, J. A. Piper, J. P. Robinson and D. Y. Jin, *Nat. Photonics*, 2014, **8**, 33–37.
24 Y. Li, J. Tang, L. He, Y. Liu, Y. Liu, C. Chen and Z. Tang, *Adv. Mater.*, 2015, **27**, 4075–4080.
25 K. Zheng, G. He, W. Song, X. Bi and W. Qin, *J. Mater. Chem. C*, 2015, **3**, 11589–11594.
26 R. Martín-Rodríguez, S. Fischer, A. Ivaturi, B. Froehlich, K. W. Krämer, J. C. Goldschmidt, B. S. Richards and A. Meijerink, *Chem. Mater.*, 2013, **25**, 1912–1921.
27 L. Cheng, C. Wang, L. Feng, K. Yang and Z. Liu, *Chem. Rev.*, 2014, **114**, 10869–10939.
28 S. Gai, C. Li, P. Yang and J. Lin, *Chem. Rev.*, 2014, **114**, 2343–2389.
29 B. Chen, T. Sun, X. Qiao, X. Fan and F. Wang, *Adv. Opt. Mater.*, 2015, **3**, 1577–1581.
30 J. Lai, B. P. Shah, Y. Zhang, L. Yang and K. B. Lee, *ACS Nano*, 2015, **9**, 5234–5245.
31 W. Xu, X. Min, X. Chen, Y. Zhu, P. Zhou, S. Cui, S. Xu, L. Tao and H. Song, *Sci. Rep.*, 2014, 4.
32 H. H. Gorris and O. S. Wolfbeis, *Angew. Chem., Int. Ed.*, 2013, **52**, 3584–3600.
33 J. Wang, R. R. Deng, M. A. MacDonald, B. L. Chen, J. K. Yuan, F. Wang, D. Z. Chi, T. S. A. Hor, P. Zhang, G. K. Liu, Y. Han and X. Liu, *Nat. Mater.*, 2014, **13**, 157–162.
34 X. Li, X. Liu, D. M. Chevrier, X. Qin, X. Xie, S. Song, H. Zhang, P. Zhang and X. Liu, *Angew. Chem., Int. Ed.*, 2015, **54**, 13312–13317.
35 Y. Wang, W. Cao, S. Li and W. Wen, *Appl. Phys. Lett.*, 2016, **108**, 051902.
36 Z. Mi, Y. Zhang, S. K. Vanga, C. B. Chen, H. Q. Tan, F. Watt, X. Liu and A. A. Bettiol, *Nat. Commun.*, 2015, **6**, 8832.
37 S. Zeng, H. Wang, W. Lu, Z. Yi, L. Rao, H. Liu and J. Hao, *Biomaterials*, 2014, **35**, 2934–2941.
38 E. M. Chan, G. Han, J. D. Goldberg, D. J. Gargas, A. D. Ostrowski, P. J. Schuck, B. E. Cohen and D. J. Milliron, *Nano Lett.*, 2012, **12**, 3839–3845.
39 F. Wang and X. Liu, *Acc. Chem. Res.*, 2014, **47**, 1378–1385.
40 W. Wei, Y. Zhang, R. Chen, J. Goggi, N. Ren, L. Huang, K. K. Bhakoo, H. D. Sun and T. T. Y. Tan, *Chem. Mater.*, 2014, **26**, 5183–5186.
41 X. Wu, H. Lee, O. Bilsel, Y. Zhang, Z. Li, T. Chen, Y. Liu, C. Duan, J. Shen, A. Punjabi and G. Han, *Nanoscale*, 2015, **7**, 18424–18428.
42 W. Q. Zou, C. Visser, J. A. Maduro, M. S. Pshenichnikov and J. C. Hummelen, *Nat. Photonics*, 2012, **6**, 560–564.

43 F. Wang and X. Liu, *J. Am. Chem. Soc.*, 2008, **130**, 5642–5643.
44 R. Deng, F. Qin, R. Chen, W. Huang, M. Hong and X. Liu, *Nat. Nanotechnol.*, 2015, **10**, 237–242.
45 A. Sedlmeier and H. H. Gorris, *Chem. Soc. Rev.*, 2015, **44**, 1526–1560.
46 J. C. Boyer, C. J. Carling, B. D. Gates and N. R. Branda, *J. Am. Chem. Soc.*, 2010, **132**, 15766–15772.
47 C. Zhang, L. Yang, J. Zhao, B. Liu, M. Y. Han and Z. Zhang, *Angew. Chem., Int. Ed.*, 2015, **54**, 11531–11535.
48 G. Chen, T. Y. Ohulchanskyy, A. Kachynski, H. Agren and P. N. Prasad, *ACS Nano*, 2011, **5**, 4981–4986.
49 M. Pollnau, D. R. Gamelin, S. R. Lüthi, H. U. Güdel and M. P. Hehlen, *Phys. Rev. B: Condens. Matter*, 2000, **61**, 3337–3346.
50 J. F. Suyver, A. Aebischer, S. García-Revilla, P. Gerner and H. U. Güdel, *Phys. Rev. B: Condens. Matter*, 2005, **71**, 125123.
51 F. Wang, R. Deng and X. Liu, *Nat. Protoc.*, 2014, **9**, 1634–1644.
52 M. T. Berry and P. S. May, *J. Phys. Chem. A*, 2015, **119**, 9805–9811.
53 X. Chen, D. Peng, Q. Ju and F. Wang, *Chem. Soc. Rev.*, 2015, **44**, 1318–1330.
54 H. Schäfer, P. Ptacek, O. Zerzouf and M. Haase, *Adv. Funct. Mater.*, 2008, **18**, 2913–2918.
55 Y. Wang, L. Tu, J. Zhao, Y. Sun, X. Kong and H. Zhang, *J. Phys. Chem. C*, 2009, **113**, 7164–7169.
56 A. Kar and A. Patra, *Nanoscale*, 2012, **4**, 3608–3619.
57 S. Han, R. Deng, X. Xie and X. Liu, *Angew. Chem., Int. Ed.*, 2014, **53**, 11702–11715.
58 F. Zhang, R. Che, X. Li, C. Yao, J. Yang, D. Shen, P. Hu, W. Li and D. Zhao, *Nano Lett.*, 2012, **12**, 2852–2858.
59 L. Lei, D. Chen, P. Huang, J. Xu, R. Zhang and Y. Wang, *Nanoscale*, 2013, **5**, 11298–11305.
60 Y. Wang, K. Liu, X. M. Liu, K. Dohnalová, T. Gregorkiewicz, X. G. Kong, M. C. G. Aalders, W. J. Buma and H. Zhang, *J. Phys. Chem. Lett.*, 2011, **2**, 2083–2088.
61 J. Zhao, Z. Lu, Y. Yin, C. McRae, J. A. Piper, J. M. Dawes, D. Jin and E. M. Goldys, *Nanoscale*, 2013, **5**, 944–952.
62 F. Vetrone, R. Naccache, V. Mahalingam, C. G. Morgan and J. A. Capobianco, *Adv. Funct. Mater.*, 2009, **19**, 2924–2929.
63 F. Wu, X. Liu, X. Kong, Y. Zhang, L. Tu, K. Liu, S. Song and H. Zhang, *Appl. Phys. Lett.*, 2013, **102**, 243104.
64 J.-C. Boyer, M.-P. Manseau, J. I. Murray and F. C. J. M. van Veggel, *Langmuir*, 2009, **26**, 1157–1164.
65 Y. P. Li, J. H. Zhang, Y. S. Luo, X. Zhang, Z. D. Hao and X. J. Wang, *J. Mater. Chem.*, 2011, **21**, 2895–2900.
66 J. M. Meruga, A. Baride, W. Cross, J. J. Kellar and P. S. May, *J. Mater. Chem. C*, 2014, **2**, 2221–2227.
67 G. Y. Chen, Y. Liu, Y. G. Zhang, G. Somesfalean, Z. G. Zhang, Q. Sun and F. P. Wang, *Appl. Phys. Lett.*, 2007, **91**, 133103.
68 Y. F. Bai, Y. X. Wang, G. Y. Peng, W. Zhang, Y. K. Wang, K. Yang, X. R. Zhang and Y. L. Song, *Opt. Commun.*, 2009, **282**, 1922–1924.
69 M. Quintanilla, F. Q. Ren, D. L. Ma and F. Vetrone, *ACS Photonics*, 2014, **1**, 662–669.
70 H. Wen, H. Zhu, X. Chen, T. F. Hung, B. Wang, G. Zhu, S. F. Yu and F. Wang, *Angew. Chem., Int. Ed.*, 2013, **52**, 13419–13423.